

FIRST X-RAY OBSERVATIONS OF THE YOUNG PULSAR J1357–6429

VYACHESLAV E. ZAVLIN

Space Science Laboratory, NASA MSFC SD59, Huntsville, AL 35805; vyacheslav.zavlin@msfc.nasa.gov
Draft version June 17, 2019

ABSTRACT

The first short *Chandra* and *XMM*-Newton observations of the young and energetic pulsar J1357–6429 provided indications of a tail-like pulsar-wind nebula associated with this object, as well as pulsations of its X-ray flux with a pulsed fraction $p_f \approx 50\%$ and a thermal component dominating at energies $E \gtrsim 2$ keV. The elongated nebula is very compact in size and might be interpreted as evidence for a pulsar jet. The thermal radiation is most plausibly emitted from the entire neutron star surface of a 10 km radius and a $10^9 - 10^{10}$ K temperature, covered with a hydrogen atmosphere. At higher energies the pulsar’s emission is of a nonthermal origin, with a power-law spectrum of a photon index $\gamma = 1.1 - 0.2$. This makes the properties of PSR J1357–6429 very similar to those of the young pulsars J1119–6127 and Vela with detected thermal radiation.

Subject headings: pulsars: individual (PSR J1357–6229) – stars: neutron — stars: X-rays

1. INTRODUCTION

Once discovered in radio, young rotation-powered pulsars with characteristic ages of $\tau_c = P/2\dot{P} \approx 10$ kyr (P is pulsar spin period) often become targets for X-ray observations because these objects usually possess large values of the rotational-energy loss, $E \gtrsim 10^{36}$ ergs s⁻¹, and hence are expected to generate observable nonthermal (magnetospheric) emission and power detectable pulsar-wind nebulae (PWNe; see Kargaltsev, Pavlov, & Garmire 2007 for properties of a number of PWNe). Measuring parameters of the magnetospheric radiation is particularly important for inferring emission processes operating in pulsar magnetosphere. Studying a PWN is essential for determining the energy of the pulsar wind, probing the ambient medium, and understanding the shock acceleration mechanism(s).

On the other hand, neutron stars (NSs), born hot in supernova explosions, cool down via neutrino emission from the entire NS body and heat transport through the stellar envelope to the surface and subsequent thermal radiation. The NS cooling rate is determined by various processes of the neutrino emission, as well as the (unknown) properties of the NS inner matter (Yakovlev & Pethick 2004). Till recently, young pulsars were thought to be such powerful nonthermal X-ray emitters that their thermal radiation would be completely buried under the nonthermal component. However, new observations revealed the pulsars Vela ($\tau_c = 11.3$ kyr) and J1119–6127 ($\tau_c = 1.6$ kyr) as examples of young NSs with the bulk of the X-ray flux of a thermal origin (Pavlov et al. 2001; Gonzalez et al. 2005). The surface emission is of a special interest because confronting observational data with model thermal radiation, presumably formed in NS atmospheres, can allow one to infer the surface temperatures and magnetic fields, constrain the NS mass (M) and radius (R), and understand the properties of the superdense matter in the NS interior (see Zavlin 2007a [hereafter Z07] for a review).

At a distance of $d \approx 2.5$ kpc derived from the pulsar dispersion measure and the Galactic electron density model of Cordes & Lazio (2002), PSR J1357–6429 ($P = 166$ ms, $\tau_c = 7.3$ kyr, $E = 3.1 \times 10^{36}$ ergs s⁻¹, surface magnetic field $B \approx 8 \times 10^{12}$ G), discovered by Camilo et al. (2004; hereafter C04) during the Parkes multibeam survey of the Galactic plane, is one of the nearest objects in the group of about

two dozen currently known pulsars¹ with $\tau_c < 15$ kyr. The actual pulsar’s age could be $\tau_c = 2 \tau_c = [n - 1] < 15$ kyr, for a typical value of the magneto-dipole braking index $n' = 2-3$. Radio data on this pulsar (C04) revealed a strong glitch of its spin period, $\dot{P} = P' - 2.4 \times 10^{-6}$, similar to those experienced by some other young pulsars (e. g., Vela), supporting the hypothesis that PSR J1357–6429 is a young NS. It is located relatively close to the supernova remnant (SNR) candidate G309.8–2.6, but a possible connection between these two objects has yet to be established (see C04 for details), opposite to the case of the majority of young pulsars associated with SNRs.

As with many other young pulsars, PSR J1357–6429 has been a target of both *Chandra* and *XMM*-Newton. Sections 2 and 3 describe these observations and analysis of the collected X-ray data. The results are discussed in Sec. 4.

2. OBSERVATIONS AND DATA REDUCTION

XMM-Newton observed PSR J1357–6429 on 2005 August 5 for 11.6 and 14.5 ks of effective exposures with the European Photon Imaging Cameras, EPIC-pn and MOS (respectively), operated in Full-Frame Window mode. The highest achieved time resolution of 73.4 ms is not sufficient for timing of a signal of a 166-ms period. The data were reprocessed with the *XMM*-Newton Science Analysis Software (SAS v. 7.0.0). Due to strong particle flares a background level during about 85% of the total observational span was higher by a factor of 3–20 than the “quiescent” rate.

The pulsar was observed with the *Chandra* High Resolution Camera (HRC-S) operated in Timing mode on 2005 November 18 and 19, for 16.1 and 17.1 ks of effective exposure and with a 16- ms time resolution. The *Chandra* Interactive Analysis of Observations (CIAO) software (v. 3.4; CALDB ver.3.3.0.1) was used to generate the level 2 event files from the two observations. Those were combined with the CIAO script ‘merge_all’, that resulted in the data product of a 33.2 ks exposure. The pulse-invariant (PI) channels with $PI < 25$ or $PI > 150$ were filtered out to minimize background contamination.

3. OBSERVATIONAL RESULTS

¹ <http://www.atnf.csiro.au/research/pulsar>

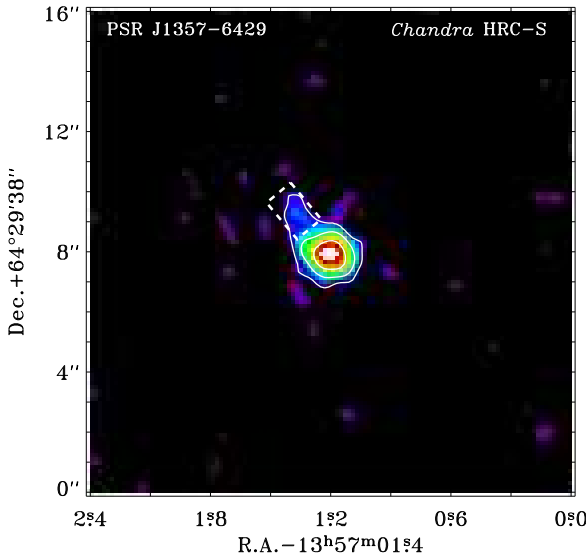


FIG. 1.— *Chandra* HRC-S $16''$ $16''$ image smoothed with a $0''\!4$ FWHM Gaussian showing PSR J1357–6429 surrounded by an extended structure elongated in the east-north direction (indicated by the white-dashed box of a $1''\!95$ size). White contours correspond to intensity values of 0.17 , 0.55 , and 1.74 counts $\text{arcsec}^{-2} \text{ks}^{-1}$.

3.1. Spatial analysis

Figure 1 presents a smoothed HRC-S image of the $16''$ $16''$ region around the radio position of PSR J1357–6429 derived by C04. The image reveals a point-like source surrounded by a weaker diffuse emission. The source is centered at the position $\text{R.A.} = 13^{\text{h}}57^{\text{m}}254$ and $\text{Dec.} = -64^{\circ}29'30''$. The difference of $0''\!74$ between the X-ray and radio positions is very close to the $1''$ error in the *Chandra* HRC-S positional astrometry². The diffuse emission feature, extending toward northeast to a distance of about $2''$ from the center of the point-like source, is seen in the both HRC-S datasets and is not an image artifact caused by the instrument anomalies and/or background³. The presence of the extended emission is also apparent in Fig. 2 showing two 1-D distributions of counts in rectangular apertures shifted along the main symmetry axis of the box plotted in Fig. 1: one histogram presents the distribution of detected counts, the other indicates the HRC-S point-spread function computed from a 2-D simulation performed with the CIAO 'mkpsf' tool. The proximity of the X-ray and radio positions and the morphology of the extended feature strongly suggest that the detected X-ray radiation is emitted by PSR J1357–6429 and its possible PWN⁴.

The $1''\!95$ $1''\!58$ box shown in Fig. 1 contains 18 counts, of them only 14% belongs to background. Hence, the elongated “tail” of the diffuse emission (within the box) emits at a rate of 0.48 ± 0.14 counts ks^{-1} . Modeling the tail’s emission with a power-law (PL) spectrum of a photon index $\gamma = 1.5$ (typical for X-ray PWNe — e. g., Kargaltsev et al. 2007) absorbed with the hydrogen column density $n_{\text{H21}} = n_{\text{H}} = (10^{21} \text{ cm}^{-2}) = 5.0$ (see Sec. 3.3) yields the tail’s (unabsorbed) flux $F_{\text{t}} \approx 3.3 \times 10^{-14} \text{ ergs cm}^{-2} \text{ s}^{-1}$ in 0.5 – 10 keV, or the luminosity $L_{\text{t}} \approx 2.5 \times 10^{31} d_{2.5}^2 \text{ ergs s}^{-1}$ ($d_{2.5} = d = [2.5 \text{ kpc}]$).

No large-scale signatures of a diffuse emission which could

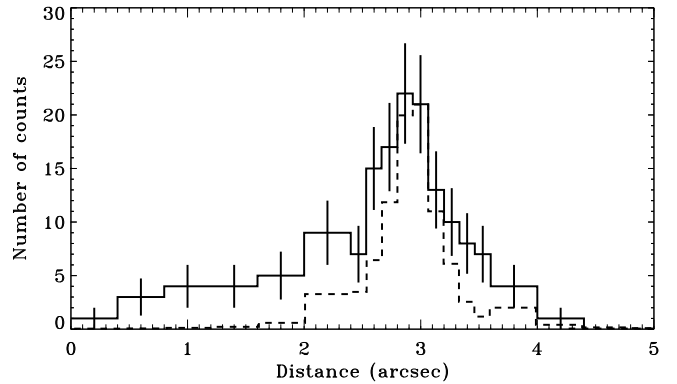


FIG. 2.— Distribution of counts detected with the *Chandra* HRC-S instrument (solid histogram) in rectangular apertures with a $1''\!84$ height and varying widths ($0''\!13$ or $0''\!40$) shifted along the main symmetry axis of the box shown in Fig. 1. The dashed histogram shows the HRC-S point-spread function computed for the same apertures.

be associated with the SNR candidate G309.8–2.6 (Sec. 1) were found in these data. An upper limit on the averaged surface brightness of the possible SNR emission, estimated from the $2''$ -radius circle centered at the position $\text{R.A.} = 13^{\text{h}}56^{\text{m}}57^{\text{s}}$ and $\text{Dec.} = -64^{\circ}28'00''$, is 5 counts $\text{ks}^{-1} \text{ arcmin}^{-2}$.

3.2. Timing analysis

For the timing analysis, 137 counts were extracted from the $1''\!05$ -radius circle centered at the pulsars X-ray position, with 132 counts estimated to belong to the pulsar. The photon times of arrival were corrected to the solar system barycenter using the CIAO ‘axBary’ tool and the pulsars radio position and convolved with the accurate timing solution obtained from radio observations of the pulsar conducted at the Parkes telescope⁵ in the interval from 2005 April 27 to 2005 December 10 (53,487–53,714 MJD): $f = 6.019298216(5)$ Hz and, $f = -1.29968(6) \times 10^{-11}$ Hz s^{-1} at the epoch 53,694.0 MJD (given with the $1''$ uncertainties; F. Camilo 2007, private communication). This radio solution leaves a timing residual of only 3.6 ms (2.2% of the spin period). At this ephemeris, the Z_m^2 -test (m is number of harmonics) results in the value of $Z_1^2 = 12.0$ ($Z_2^2 = 14.6$), or a signal detection at a 99.752% confidence level.

Figure 3 presents the pulse profile of PSR J1357–6429 extracted at the radio spin parameters, with the estimated pulsed fraction, $p_f = 63 \pm 15\%$ (defined as the fraction of counts above the minimum in the light curve). The χ^2 -test yields the value $\chi^2 = 4.07$ for 9 d.o.f, meaning a 95.996% probability that the pulse profile differs from a constant line. Because of the poor statistics, the shape of the pulse profile is not well determined. The only rather certain fact is that the pulsed fraction is large, implying special properties of the detected X-ray emission (see Sec. 4).

3.3. Spectral analysis

To optimize the signal-to-noise ratio, the EPIC spectra were extracted from $20''$ -radius circles centered at the pulsar position (these include the emission of the faint PWN suggested by the HRC-S data). The extraction regions contain about

² <http://asc.harvard.edu/cal/ASPECT/celmon>

³ <http://cxc.harvard.edu/proposer/POG/html/HRC.html>

⁴ No other point-like source as a possible counterpart of this feature is found in available observational catalogues.

⁵ The Parkes Observatory is part of the Australia Telescope, which is funded by the Commonwealth of Australia for operation as a National Facility managed by CSIRO.

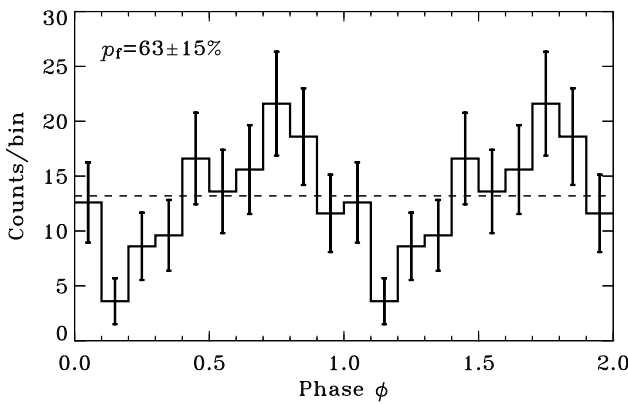


FIG. 3.— Pulse profile of PSR J1357–6429 extracted from the *Chandra* HRC-S data. The dashed line indicates the mean level.

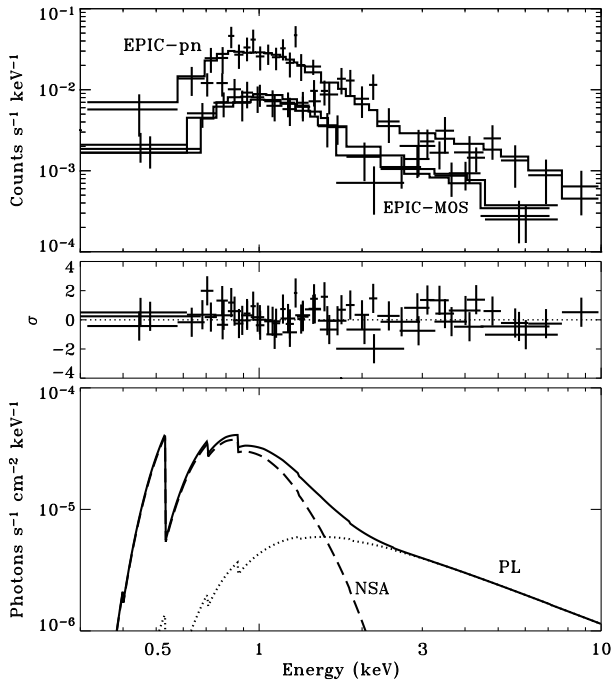


FIG. 4.— Spectra of PSR J1357–6429 detected with the XMM-Newton EPIC instruments and fitted with a two-component, NS atmosphere (NSA) plus power law (PL), model.

75% of the source flux. The instrumental responses were generated with the SAS ‘rmfgen’ and ‘arfgen’ tools. Background was evaluated from similar regions in vicinity of the pulsar position. The estimated source count rates (corrected for the finite extraction aperture) are 56 \pm 5 and 17 \pm 2 counts ks^{-1} in 0.3–10 keV, for EPIC-pn and MOS, respectively.

A single PL model fits the spectra rather well, with $\text{min}^2 = 1.17$ for $\nu = 59$ d.o.f, yielding $\nu = 2.1 \pm 0.4$ and $n_{\text{H},21} = 2.3 \pm 0.8$ (1 σ errors are given here and below). The derived non-thermal (isotropic) luminosity in 0.5–10 keV is $L_{\text{nonth}} = 2.0 \times 10^{32} d_{2.5}^2 \text{ ergs s}^{-1} = 6.5 \times 10^{-5} E d_{2.5}^2$ (of this, about 10% belongs to the PWN). On the other hand, it is reasonable to assume that PSR J1357–6429 emits observable thermal radiation. Adding a thermal component improves the fit, $\text{min}^2 = 0.76$ for $\nu = 57$ d.o.f, indicating that it is required by the data at a

99.9998% (4.8 σ) confidence level. The thermal component can be equally well described with both a blackbody (BB) spectrum and a NS magnetized ($B = 1 \times 10^{13}$ G) hydrogen atmosphere model⁶. However, as in many other cases, the estimates on the temperature and size of the emitting area derived from these two models are very different (see Zavlin 2007a for details): $T_{\text{bb}}^1 = 1.7 \pm 0.2$ MK and $R_{\text{bb}}^1 = (2.5 \pm 0.5) d_{2.5}$ km (redshifted values) in the BB fit, and $T_{\text{eff}} = 1.0 \pm 0.1$ MK (effective temperature) for $R = 10$ km at $d_{2.5} = 1$ in the NS atmosphere fit. The corresponding bolometric luminosities are $L_{\text{bb}}^1 = 3.7 \times 10^{32} d_{2.5}^2 \text{ ergs s}^{-1}$ and $L_{\text{atm}} = 7.1 \times 10^{32} \text{ ergs s}^{-1}$ ($L_{\text{atm}}^1 = [1 - 2GM/c^2R]L_{\text{atm}} = 0.6L_{\text{atm}}$ for $M = 1.4M_{\odot}$ and $R = 10$ km). The parameters of the nonthermal component are similar, $\nu = 1.3 \pm 0.2$ and 1.1 ± 0.2 , in the BB and atmosphere fits (respectively), with $L_{\text{nonth}} = 1.4 \times 10^{32} d_{2.5}^2 \text{ ergs s}^{-1} = 4.5 \times 10^{-5} E d_{2.5}^2$. The inferred hydrogen column density, $n_{\text{H},21} = 4.9 \pm 2.0$, is somewhat larger than in the single-PL interpretation but still consistent with the standard estimate suggested by the pulsar dispersion measure $\text{DM} = 127.2 \text{ cm}^{-3} \text{ pc}$, $n_{\text{H},\text{DM}} = (10^{21} \text{ cm}^{-2}) = \text{DM} = (10^{20} \text{ cm}^{-2}) = 4.0$ (assuming a 10% ionization degree of the interstellar hydrogen), and is reasonably lower than the galactic neutral hydrogen density estimated in the direction to PSR J1357–6429, $n_{\text{HI}} = (10^{21} \text{ cm}^{-2}) = 10.0$. It is also worth mentioning that the thermal component contributes 72% of the X-ray flux observed at $E < 2$ keV, regardless of whichever model is used to describe the component. The best two-component fit involving the NS atmosphere model is shown in Fig. 4.

4. DISCUSSION

The first X-ray observations of PSR J1357–6429 have revealed interesting properties of this object, including the indication of the compact tail-like PWN associated with the pulsar. The estimated efficiency with which PSR J1357–6429 powers the PWN, $L_{\text{t}} = E = 0.8 \times 10^{-5}$, can be considered as ‘medium’ among those measured for tail-like PWNe associated with other pulsars. For example, it is lower by about an order of magnitude than the efficiencies of the PWNe of the young pulsar B1757–24 (Kaspi et al. 2001) and the millisecond pulsar B1957+20 (Stappers et al. 2003; Zavlin 2007b) but larger by a factor of a few than those inferred for the Geminga’s tail (Pavlov, Sanwal, & Zavlin 2006) and the Vela’s southeast jet (Pavlov et al. 2003). On the other hand, the derived luminosity of the PWN associated with PSR J1357–6429 is about by a factor of 5–8 smaller than the nonthermal luminosity emitted by the pulsar itself, that does not match the correlation, $L_{\text{PWN}} \propto 5L_{\text{nonth}}$, inferred by Kargaltsev et al. (2007) for a sample of pulsars. It is premature to make firm conclusions about the properties of the possible PWN. However, despite the fact that the proper motion of PSR J1357–6429 has yet not been measured, the shape and estimated luminosity of this elongated feature may suggest a hypothesis that it is a pulsar jet along the pulsar spin axis aligned with its velocity, similar to the interpretation proposed for the tail-like features of the Crab, Vela, and Geminga pulsars (Weisskopf et al. 2000; Pavlov et al. 2003; Pavlov et al. 2006). On the other hand, if the elongation direction and that of the proper motion turn out to be perpendicular to each other, it would indicate that the X-ray emission of the PWN emerges from a torus associated with the equatorial pulsar wind. Future measurement of the pulsar proper motion is important for validating this hypotheses.

⁶ The ‘nsa’ code in the XSPEC package.

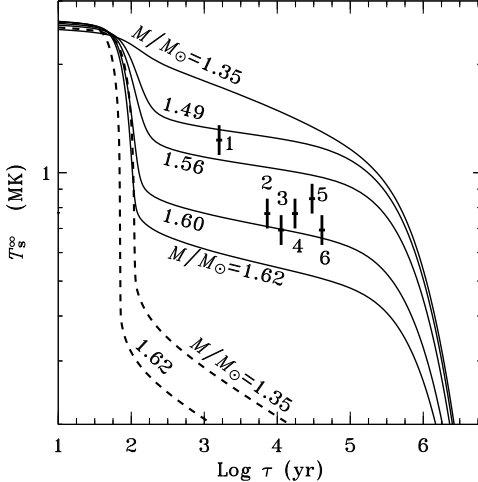


FIG. 5.— NS cooling models (Yakovlev & Pethick 2004) with the ‘2p’ proton superfluidity (solid curves) and without the superfluidity (dashed curves), for different NS masses. The crosses indicate the pulsars: J1119–6127 (1), J1357–6429 (2), Vela (3), B1706–44 (4), J0538+2817 (5), and B2334+61 (6). The redshifted surface temperature is $T_s^* = [1 - 2GM/c^2R]^{1/2}T_{\text{eff}}$ ($= 0.77T_{\text{eff}}$ for $M = M_{\odot} = 1.4$ and $R = 10$ km), with T_{eff} being the effective temperature of the NS surface obtained in the fits with the NS atmosphere models.

The spectral data on PSR J1357–6429 show that the bulk of the pulsar X-ray flux is probably of a thermal origin. It makes this object the second youngest NS in the group of energetic pulsars with a thermal component dominating at $E \approx 2$ keV. In addition to PSRs J1119–6127, J1357–6429 and Vela, the group also includes PSRs B1706–44 with $\tau_c = 17.5$ kyr, J0538+2817 with the derived true age $\tau_c = 20.5 = 30$ kyr (Kramer et al. 2003), and B2334+61 with $\tau_c = 40.9$ kyr (see Z07 for details). Similar to the situation with other members of this group, the origin of thermal component of PSR J1357–6429 cannot be unambiguously determined from the spectral data alone. The parameters of the thermal component obtained in the BB fit may be interpreted as radiation from a small hot area (polar caps) on the NS surface, although the estimated radius, $R_{\text{bb}}^1 \approx 2.5$ km, is much greater than the canonical polar cap estimate, $R_{\text{pc}} = (2\pi R^3/cP)^{1/2} \approx 0.3$ km. Opposite to this, the fit with the magnetized NS atmosphere models indicate that the thermal emission originates from the entire NS surface. One could discriminate between these two interpretations invoking pulsations of the X-ray emission. In the case of PSR J1357–6429, as the *Chandra* HRC-S instrument is most efficient at $E \approx 2$ keV, the pulsed fraction of $p_f \approx 50\%$

⁷ This assumption should be taken with caution — see the case of PSR J0538+2817.

suggests that the thermal emission is intrinsically anisotropic, as predicted by the NS atmosphere models — otherwise the effect of strong gravitational bending of photon trajectories near the NS surface would strongly suppress the pulsations. This obviously contradicts the simplistic (isotropic) BB interpretation. Such a pulsed fraction also indicates that the NS has a strong nonuniformity of the surface temperature and magnetic field. Hence, the temperature T_{eff} inferred from the NS atmosphere fit assuming the uniform surface should be considered as an approximate estimate on the “mean” surface temperature. The same conclusions stand for PSR J1119–6127 with a pulsed fraction $p_f \approx 60\%$ (Gonzalez et al. 2005), as well as PSR 0538+2817 whose pulse profile of the thermal flux emission shows a complicate dependence on photon energy (Zavlin & Pavlov 2004).

Assuming that the characteristic ages of the five pulsars of this group are close to the true ones⁷, it is illustrative to compare NS cooling models with the surface temperatures estimated for these objects from the NS atmosphere fits. Figure 5 presents cooling models with and without proton (‘2p’ model) superfluidity in the NS core (Yakovlev & Pethick 2004), as well as the measured temperatures. The superfluidity reduces the neutrino emission by suppressing the Urca processes and, hence, decelerates the NS cooling. This effect depends on NS mass, being stronger for higher masses. The comparison suggests that the interiors of these six pulsars are superfluid, and the NS masses may be in the range $M = [1.5–1.6]M_{\odot}$ (note that this range would be different for another model superfluidity).

However, despite the important X-ray information on PSR J1357–6429 available, the pulsar’s properties remain yet rather uncertain because of the scanty number of photons detected in these short exposures. Therefore, deeper observations are required to provide data of much better quality to firmly establish the actual shape, size, and spectrum of the possible PWN, and accurately infer the X-ray spectral and temporal properties of the pulsar.

The author thanks Fernando Camilo for providing the pulsar radio ephemeris and remarks to the manuscript, Dmitry Yakovlev for making available the NS cooling models, and Allyn Tennant and Martin Weisskopf for useful discussions. This work is supported by a NASA Senior Associateship Award at the NASA MSFC.

REFERENCES

Camilo, F., et al. 2004, ApJ, 611, L25 (C04)
 Cordes, J. M., & Lazio, T. J. W. 2002, preprint (astro-ph/0207156)
 Gonzalez, M. E., Kaspi, V. M., Camilo, F., Gaensler, B. M., & Pivovaroff, M. J. 2005, ApJ, 630, 489
 Kargaltsev, O. Y., Pavlov, G. G., & Garmire, G. P. 2007, ApJ, 660, 1413
 Kaspi, V. M., Gotthelf, E. V., Gaensler, B. M., & Lyutikov, M. 2001, ApJ, 562, L163
 Kramer, M., Lyne, A. G., Hobbs, G., Löhmer, O., Carr, P., Jordan, C., & Wolszczan, A. 2003, ApJ, 593, L31
 Pavlov, G. G., Zavlin, V. E., Sanwal, D., Burwitz, V., & Garmire, G. P. 2001, ApJ, 552, L129
 Pavlov, G. G., Teter, M. A., Kargaltsev, O. Y., & Sanwal, D. 2003, ApJ, 591, 1157
 Pavlov, G. G., Sanwal, D., & Zavlin, V. E. 2006, ApJ, 643, 1146
 Stappers, B. W., Gaensler, B. M., Kaspi, V. M., van der Klis, M., & Lewin, W. H. G. 2003, Science, 299, 1372
 Yakovlev, D. G., & Pethick, C. J. 2004, ARA&A, 42, 169
 Weisskopf, M. C., et al. 2000, ApJ, 536, L81
 Zavlin, V. E., & Pavlov, G. G. 2004, Mem.S.A.It., 75, 458
 Zavlin, V. E. 2007a, in The 363-nd Heraeus Seminar on Neutron Stars and Pulsars, Springer Lecture Notes, in press (Z07; astro-ph/0702426)
 Zavlin, V. E. 2007b, Ap&SS, 308, 297